

Atomic structure of a stripe phase on Al₂O₃/Ni₃Al(111) revealed by scanning force microscopySebastian Gritschneider,¹ Stefan Degen,² Conrad Becker,² Klaus Wandelt,² and Michael Reichling^{1,*}¹Fachbereich Physik, Universität Osnabrück, BarbarasträÙe 7, 49076 Osnabrück, Germany²Institut für Physikalische und Theoretische Chemie, Universität Bonn, Wegelerstraße 12, 53115 Bonn, Germany

(Received 26 March 2007; revised manuscript received 3 July 2007; published 30 July 2007)

The most remarkable feature of the ultrathin aluminum oxide film grown on Ni₃Al(111) as reported in the literature is its surface reconstruction resulting in a dot structure with a large rhombic surface unit cell. Here, we demonstrate that this is the reconstruction of the dominant phase of the oxide film, while 5%–20% of the surface area may be covered by another reconstruction that is characterized by zigzag features arranged in parallel stripes. When investigated with scanning tunneling microscopy, this stripe phase appears to be very different from the dominant phase; however, highest resolution dynamic scanning force microscopy operated in the noncontact mode reveals great similarity of the atomic structures. Both phases consist of a modulated hexagonal lattice with 0.51 nm periodicity resembling the aluminum sublattice of the Ni₃Al(111) substrate.

DOI: [10.1103/PhysRevB.76.014123](https://doi.org/10.1103/PhysRevB.76.014123)

PACS number(s): 68.37.Ps, 68.47.Gh

INTRODUCTION

Alumina surfaces are of great interest in a variety of applications, for example, as substrates in heterogeneous catalysis,¹ as high- κ gate dielectrics in microelectronics,² or as protective coatings of metallic assemblies against environmental influences.³ For an in-depth understanding of the role of alumina in these applications as well as for the development and tailoring of its properties, a detailed knowledge of the surface structure down to the atomic level is inevitable. This is particularly needed for nanostructures that are used as templates for the self-assembled growth of metal cluster arrays.^{4,5} The creation of arrays of monodisperse metal clusters is of great interest in the context of model studies in catalysis research and the ultrathin aluminum oxide film grown on a Ni₃Al(111) alloy substrate⁶ has been shown to be well suited for such studies. Its previously observed reconstruction revealing a perfectly regular dot superstructure can be used for the controlled formation of metallic nanoclusters ordered on a regular grid.^{7,8} Consisting of only two oxide layers,⁹ the film is thin enough to provide conductivity for being investigated by electron based surface analysis techniques. Recently, the nanoscopic superstructures of the oxide film have been investigated with spot profile analysis low energy electron diffraction and scanning tunneling microscopy (STM),¹⁰ while dynamic scanning force microscopy (SFM) operated in the noncontact mode revealed that the superstructure is built up by a modulated hexagonal lattice with 0.29 nm interatomic distance.¹¹

In this paper, we demonstrate that the hitherto observed dot structure is the reconstruction of the *dominant phase* of the oxide film and we report on a new phase that we further on refer to as the *stripe phase* as it is composed of parallel aligned zigzag shaped stripes. Applying a well proven preparation recipe, the stripe phase is found to coexist with the dominant phase and claims 5%–20% of the surface area. In STM measurements performed at low temperature, the stripe phase appears very different from the dominating phase. However, we demonstrate with highly resolved SFM measurements that both phases are built up by the same structural elements, which are arranged on the substrate in a simi-

lar manner. Although, their unit cells have different sizes and orientations, both phases are composed of hexagons with 0.29 nm side length pinned to the 0.51 nm periodicity aluminum sublattice of the Ni₃Al(111) substrate.

EXPERIMENT

Experiments were performed in two different ultrahigh vacuum chambers, each having a base pressure below 2×10^{-8} Pa. STM and scanning tunneling spectroscopy (STS) measurements were performed at 23 K with a homebuilt setup based on a beetle-type STM operated in a liquid helium cooled cryostat.¹² For STS measurements, we fed a voltage proportional to the tunnel current I_t to a lock-in amplifier to determine the differential conductance dI_t/dU_B as a function of the tunneling bias voltage U_B . This quantity represents the sample density of states convoluted with the tip density of states; however, for the latter we assume that it does not exhibit any significant structure in the voltage range covered by our experiments. A modulation frequency of 10 kHz and an amplitude of 60 mV were applied.

For SFM, we used a commercial instrument operated at room temperature in the so-called constant-height mode, which proved to yield highest resolution images on clean insulating oxide surfaces.^{13,14} A bias voltage from -0.3 to -1.0 V was applied between the sample and the tip to compensate electrostatic forces due to charges present at the surface. The tip and the cantilever (NanoWorld AG, Neuchâtel, Switzerland, PPP-QFMR, $f_0=70$ kHz, $Q>30\,000$) were cleaned by heating them to 120 °C for several hours prior to performing experiments.

The polished Ni₃Al(111) single crystal (MaTeck, Jülich, Germany) was prepared by repeated cycles of Ar⁺-ion sputtering at a sample temperature of 600 K (5–20 min, 2.5 keV, 9.5 $\mu\text{A cm}^{-2}$) with subsequent annealing at 1150 K (7 min) and 1000 K (7 min), respectively. Alumina films were grown *in situ* by oxidation of the clean surface at 1000 K at an oxygen partial pressure of 3×10^{-6} Pa. After an O₂ exposure of 40 L (1 L = 10^{-6} Torr s), dosing was stopped, and the sample was annealed at 1050 K for 5 min. This oxidation process was performed two times to obtain a closed

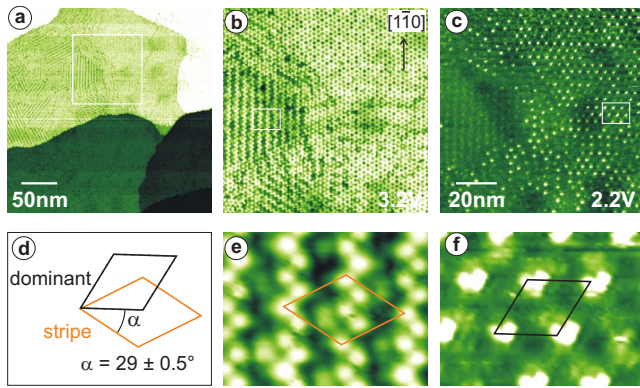


FIG. 1. (Color online) (a) STM image of the ultrathin alumina film on $\text{Ni}_3\text{Al}(111)$ showing the coexistence of the dominant and stripe phases (bias voltage=3.2 V, tunneling current=95 pA, temperature=23 K). (b) Magnification of the square area marked in (a). In the upper right half of this frame, the dominant phase is visible that appears as the hexagonal pattern of the network structure, while in the lower left half of the frame, the zigzag structures of the stripe phase are found. Stripes run parallel to one of the $[1\bar{1}0]$ directions of the network structure of the dominant phase. (c) Same area as in (b) but imaged at a bias voltage of 2.4 V. The changed imaging conditions result in the appearance of the dominant phase as the dot structure rather than the network structure and the contrast of the stripe pattern almost vanishes. Frames (e) and (f) are taken from the marked areas of frames (b) and (c) and demonstrate in higher magnification structural details of the stripe and dominant phases, respectively. (d) The rhombuses drawn in red and black denote the respective unit cells including an angle of 29° .

alumina film with a high degree of long-range order.

STM IMAGING

In Fig. 1(a), a typical large scale STM image of the oxide film is shown. The surface exhibits atomically flat terraces with a width of several hundred nanometers that are separated by steps with a height of multiples of 0.2 nm corresponding to the monolayer height of the substrate.¹⁵ We find that monolayer steps are often bunched in triples and most observed step heights are multiples of 0.6 nm.

Frame (b) is a magnification of the square area marked in frame (a) recorded by applying the same tunneling conditions. The regular patterns of two different surface reconstructions can clearly be recognized. In the upper right half of this frame, the symmetric pattern of the dominant phase is visible that appears in the *network structure* at a tunneling bias of 3.2 V. In the lower left half of the frame, a new phase, further on referred to as the stripe phase, is found, which is a structure with long-range order in the form of bright spots arranged in zigzag stripes having a distance of 3.9 nm. Stripes are found in three different directions enclosing angles of 60° and 120° and run parallel to one of the $[1\bar{1}0]$ directions of the network structure.

Switching the tunneling bias voltage to 2.2 V changes the appearance of the surface structure dramatically, as demonstrated in Fig. 1(c). Due to an additional electronic state in the band gap of the oxide film, the dominant phase appears

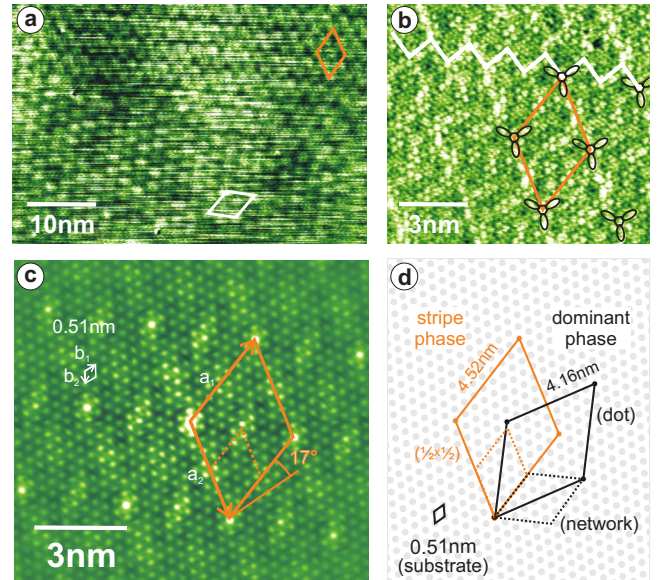


FIG. 2. (Color online) (a) SFM image of a surface area exhibiting the dominant phase (lower part, white unit cell) and the stripe phase (upper part, red unit cell). This image was slightly smoothed to highlight the two phases. (b) High resolution dynamic SFM image of the stripe phase area. The stripes (highlighted zigzag line) are mainly formed by propeller-shaped structures marking the corners of the surface unit cell. (c) Autocorrelation of frame (b) emphasizing the main periodicities of the image. The brightest features are the points of highest correlation defining the surface unit cell (solid red rhomb). Additionally, less pronounced contrast features define a $(1/2 \times 1/2)$ substructure unit cell (dashed red rhomb). Also, a 0.51 nm periodicity is found that is related to the unit cell of the $\text{Ni}_3\text{Al}(111)$ substrate. (d) Schematic representation of the relations between the substrate lattice and the unit cells of the stripe and of the dominant phase. Each phase exhibits a substructure (dashed rhombi) that are similar in size and modulate the atomic lattice.

in the *dot structure*, which is a $(\sqrt{3} \times \sqrt{3})R30^\circ$ superstructure of the network structure.¹⁰ On the contrary, the contrast of the stripe vanishes almost completely, which can be understood by the results of STS experiments discussed in detail below. As there is no difference in apparent heights between bright features of the stripe phase and those of the network structure of the dominant phase [Fig. 1(b)], we anticipate that the stripe phase also represents a double layer alumina film. In the lower frames of Fig. 1, we show the unit cells [frame (d)] and details of the stripe phase [frame (e)] and the dominant phase [frame (f)]. The unit cell of the stripe phase ($a_{\text{stripe}} = 4.52 \pm 0.05$ nm) is slightly larger than that of the dominant phase ($a_{\text{dominant}} = 4.16 \pm 0.05$ nm) and the unit cells are rotated by an angle of $29.0^\circ \pm 0.5^\circ$ with respect to each other.

SFM IMAGING

Atomic details of the stripe phase can be revealed by SFM imaging. Figure 2(a) represents a SFM image of a surface area that exhibits both phases. In the upper half of Fig. 2(a), the oxide film adopts the stripe phase, while the dominant

phase is present in the lower half. Figure 2(b) shows an area of the stripe phase with higher magnification and reveals a highly complex atomic structure. At this scale, the stripes are hardly visible anymore but we highlighted them by the white zigzag line. Instead, the prominent features are propellerlike formations (marked in black) that define the corners of the rhombic unit cell.

The identification of the stripe phase unit cell becomes especially evident from the self-correlation image shown in Fig. 2(c). The unit cell is defined by the points of strongest autocorrelation. In this frame, we furthermore find an enhanced contrast for a group of hexagonally arranged spots defining a $(1/2 \times 1/2)$ substructure of the unit cell with a relevance discussed below. The self-correlation image also clearly reveals a hexagonal 0.51 nm grid that has also been found for the dominant phase where it has been associated with the unit cell of the Ni₃Al(111) alloy surface ($a_{sub} = 0.5076$ nm).¹⁵ In our previous study, we found that the unit cell of the dominant phase is commensurate with the 0.51 nm periodicity.¹¹ Remarkably, we find that the unit cell of the stripe phase is also commensurate with this periodicity and determine the following transformation matrix from our images:

$$\begin{pmatrix} a_1 \\ a_2 \end{pmatrix}_{\text{stripe}} = \begin{pmatrix} 7 & -3 \\ 3 & 10 \end{pmatrix} \begin{pmatrix} b_1 \\ b_2 \end{pmatrix}_{0.51 \text{ nm}}$$

[In Wood notation: $(\sqrt{79} \times \sqrt{79})R17^\circ$].

The schematic representation of frame (d) brings together the unit cells of the substrate (black, solid, 0.51 nm), the stripe phase (red, solid, 4.52 nm), and the dominant phase (black, solid, 4.16 nm). Additionally, we depict with dashed rhombuses the unit cells of the substructures. For both phases, the 0.51 nm structure is not commensurate with the substructures in the first order but in the second and third orders, respectively. To reveal further details of the periodic structures of the stripe phase, we performed a Fourier transformation of the highly resolved SFM image from Fig. 2(b). The resulting Fourier power spectrum, shown in Fig. 3, in general resembles the Fourier spectrum of the dominant phase.¹¹ All reflexes are arranged on a hexagonal grid with a nearest neighbor distance of $a_{nn}^* = (4.5 \text{ nm})^{-1}$ in the reciprocal space corresponding to the real space surface unit cell and they can, therefore, be explained as higher order reflexes of this structure.

Among the multitude of spots, strong hexagonally arranged reflexes clearly mark the 0.51 nm periodicity. These reflexes are rotated by $17.0^\circ \pm 0.5^\circ$ with respect to the reflexes of the stripe phase. The outermost reflexes are groups of five spots, indicating a further periodic structure with a dimension of 0.29 nm. The main spots of these groups marked by solid black circles represent a $(1/\sqrt{3} \times 1/\sqrt{3})R30^\circ$ substructure of the 0.51 nm periodicity. The additional linearly arranged reflexes marked by gray circles are satellites indicating a modulation of the 0.29 nm lattice. The modulating structure is given by the translation vector between the satellites. Here, this vector is $2a_{nn}^*$, which means that the 0.29 nm lattice is modulated by the $(1/2 \times 1/2)$ substructure of the stripe phase. In this sense, the $(1/2 \times 1/2)$

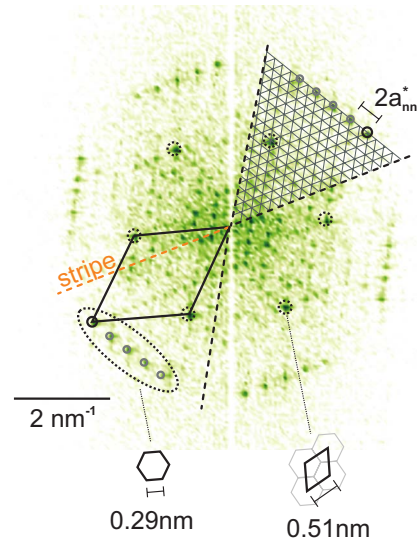


FIG. 3. (Color online) Fourier power spectrum of the SFM image from Fig. 2(b). All reflexes are arranged on a hexagonal grid corresponding to the periodicity of the stripe phase unit cell. Strong spots indicate the 0.51 nm structure of hexagons that is commensurate with the surface unit cell (dotted circles). The outermost group of strong reflexes (black solid circles) indicates the 0.29 nm periodicity of the hexagon side length. The satellites (gray solid circles) are caused by a modulation of the 0.29 nm lattice by a hexagonal lattice that is a $(1/2 \times 1/2)$ substructure of the stripe phase and its reciprocal lattice constant amounts to $2a_{nn}^*$.

substructure is equivalent to the network structure that causes the modulation of the 0.29 nm lattice of the dominant phase.¹¹

To assign real space structures to the detected periodicities, we show in Fig. 4 an average image of equally sized sections of the frame from Fig. 2(b) containing a single surface unit cell. Averaging enhances the image contrast and allows a more reliable identification of structures than it is possible from the original frames. The eye-catching features are the propeller-shaped structures defining the corners of the

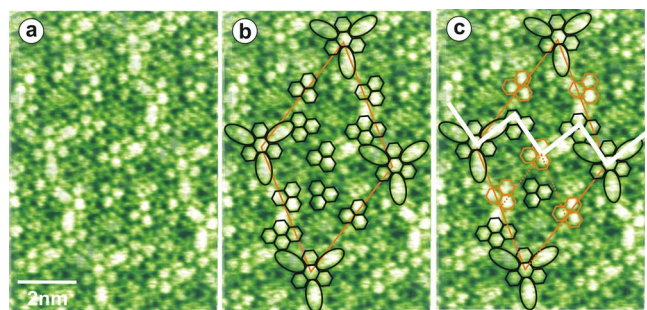


FIG. 4. (Color online) (a) Superposition of equivalent sections of Fig. 2(b) revealing structural details of the surface unit cell. For clarity, we show the resulting image (a) without and (b) with the identified hexagonal structures. The edges of the rhombic unit cell are defined by propeller-shaped features with threefold symmetry. Additionally, we find small clusters of hexagons, that are sized and oriented as predicted by the Fourier power spectrum from Fig. 3. (c) Clusters that are colored in red define the $(1/2 \times 1/2)$ substructure. Stripes are formed by the propeller features and nearby clusters.

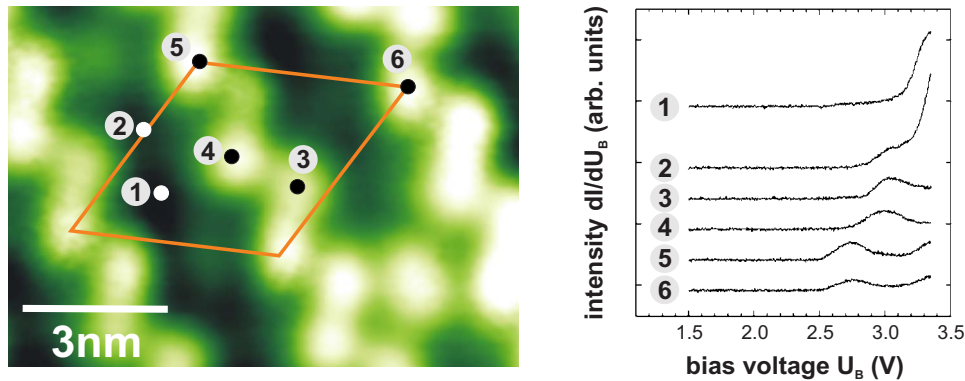


FIG. 5. (Color online) (a) STM image of the stripe phase recorded at a tunneling bias voltage of 3.2 V. At six characteristic points [between stripes (1 and 2), on the stripes (3 and 4), and on the edges of the unit cell (5 and 6)] of the unit cell, we performed scanning tunneling spectroscopy (STS) measurements. (b) STS spectra corresponding to the indicated points show the derivative of the tunneling current plotted against the tunneling bias voltage. For better clarity, curves have been shifted vertically. Characteristic features in the electronic structure are broad and rather close to each other so that a typical STM image is always composed of contributions from the unit cell, the $(1/2 \times 1/2)$ substructure, and the stripe structure.

rhombic unit cell. The center of each propeller is a bright feature that is hexagonally surrounded by six dark spots. The orientation and size of the hexagon formed by these dark spots correspond exactly to the hexagonal lattice that is indicated by the outermost spots of the Fourier power spectrum. Attached at three sides are further hexagons that are identical to the central one, while at the other sides bright ellipses form the propellerlike structure with threefold symmetry. The ellipses have the size of two hexagons but cannot be further resolved. We identify further hexagonal structures that are highlighted in Fig. 4(b). The 0.29 nm lattice does not appear as a space filling grid over the complete unit cell, but appears at some positions inside the unit cell in the form of small clusters of three or four hexagons. We demonstrate with the highlighting in Fig. 4(c) that the clusters are not located at random positions within the unit cell. The stripes are formed by adjacent clusters marked in black that cross-connect corners of the unit cell. The red colored clusters define the $(1/2 \times 1/2)$ substructure of the unit cell causing the modulation of the surface layer. Clusters are connected to each other by distorted hexagonal structures where the distortion is an effect of the modulation.

STS RESULTS

From a comparison of highly resolved images of the stripe phase and of the dominant phase, we find that the size and orientation of the 0.51 and 0.29 nm periodicities are identical for both phases, namely, both are firmly coupled to the substrate alloy structure. Therefore, we suggest that the differences between the phases do not stem from differences of the elementary structures of the oxide itself, but are caused by subtleties of the oxide-substrate interaction. In this context, we note that STM allows imaging of the well ordered aluminum sublattice of the substrate underneath the dominant phase,¹⁰ however, we never managed imaging of an ordered substrate underneath the stripe phase.

The structural similarity of the dominant and the stripe phase is further corroborated by an analysis of the electronic

structure as extracted from STS experiments. Such measurements were performed at distinct locations within the surface unit cell of the stripe phase, as shown in Fig. 5. The set of spectra measured comprises dark regions in between the stripes (spectra 1 and 2) and bright spots located on stripes (spectra 3–6) and can be subdivided into two groups revealing different electronic configurations. A negligible density of states is found for all spectra below a tunneling voltage of 2.5 V, which readily explains the observation of vanishing contrast for imaging at a tunneling voltage of 2.2 V [see Fig. 1(c)]. A common feature of spectra 1–4 is a more or less well expressed feature appearing at 3 V or at slightly higher voltage partly merging with the conduction band edge that can clearly be identified in STS measurements over a larger range of voltages.¹⁶

Most importantly, we note that there is a distinct feature at 2.75 V exclusively in spectra 5 and 6, both corresponding to points defining the surface unit cell. We further note that the feature found at point 4 defining the $(1/2 \times 1/2)$ substructure is closest to but clearly separated from the 2.75 V feature. This is in perfect agreement with STS spectra taken at points of the dominant phase where a distinct feature located at 2.4 V gives rise to the pattern of enhanced contrast defining the dot structure.¹⁶ These findings provide a clear interpretation for the differences in STM contrast formation of the dominant and stripe phases. While characteristic features of the electronic structure defining the dot and network structures of the dominant phase are well separated on the tunneling voltage scale, they are very close to each other in the case of the stripe phase. Therefore, STM images of the stripe phase exhibiting reasonable contrast are always composed of contributions from electronic states corresponding to points defining the surface unit cell (equivalent to the dot structure of the dominant phase) and others giving rise to the zigzag structure (equivalent to the network structure of the dominant phase).

CONCLUSIONS

Having investigated both phases of the ultrathin alumina film on $\text{Ni}_3\text{Al}(111)$ in detail, we find a strong correlation

between the structures of the dominant phase and that of the stripe phase despite their distinctly different morphologies apparent in large scale scanning probe microscopy images. Both structures are built up from a modulated lattice of open hexagons with a side length of 0.29 nm and the center points of the hexagons are pinned to the 0.51 nm lattice of the substrate. While the unit cells of both phases are commensurate in the first order with the substrate lattice, we find for both phases sub-structures, namely, a $(1/\sqrt{3} \times 1/\sqrt{3})R30^\circ$ (network structure) for the dominant phase and a $(1/2 \times 1/2)$ structure for the stripe phase, that are not commensurate in the first order with the substrate but modulate the atomic surface layer. It will be interesting to study whether the distinct dots defining the unit cell for the stripe phase

yield a template behavior that is similar to the one found for the dominant phase. Provided a variation in preparation conditions would allow the selective growth of one of the phases, this system could provide the highest regularity template structures that can be switched to two different lattice constants.

ACKNOWLEDGMENTS

Financial support from the Deutsche Forschungsgemeinschaft is gratefully acknowledged. We are indebted to Georg Kresse, Wolfgang Moritz, Michael Schmid, and Peter Varga for most stimulating discussions.

*reichling@uos.de

- ¹A. K. Santra and D. W. Goodman, *J. Phys.: Condens. Matter* **15**, R31 (2003).
²G. D. Wilk, R. M. Wallace, and J. M. Anthony, *J. Appl. Phys.* **89**, 5243 (2001).
³P. S. Sidky and M. G. Hocking, *Br. Corros. J.*, London **34**, 171 (1999).
⁴H. Brune, M. Giovannini, K. Bromann *et al.*, *Nature (London)* **394**, 451 (1998).
⁵N. Berdunov, G. Mariotto, K. Balakrishnan *et al.*, *Surf. Sci.* **600**, L287 (2006).
⁶U. Bardi, A. Atrei, and G. Rovida, *Surf. Sci.* **268**, 87 (1992).
⁷S. Degen, C. Becker, and K. Wandelt, *Faraday Discuss.* **125**, 343 (2004).
⁸C. Becker, A. Rosenhahn, A. Wiltner *et al.*, *New J. Phys.* **4**, 75

(2002).

- ⁹O. Bikondoa, in *Zientzia Fakultatea-Elektrika eta Elektronika Saila* (Euskal Herriko Unibertsitatea, Bilbao, 2003), p. 229.
¹⁰S. Degen, A. Krupski, M. Kraj *et al.*, *Surf. Sci.* **576**, L57 (2005).
¹¹S. Gritschneider, C. Becker, K. Wandelt *et al.*, *J. Am. Chem. Soc.* **129**, 4925 (2007).
¹²B. C. Stipe, M. A. Rezaei, and W. Ho, *Rev. Sci. Instrum.* **70**, 137 (1999).
¹³C. Barth and M. Reichling, *Nature (London)* **414**, 54 (2001).
¹⁴S. Gritschneider, Y. Namai, Y. Iwasawa *et al.*, *Nanotechnology* **16**, S41 (2005).
¹⁵M. Hansen and K. Anderko, *Constitutions of Binary Alloys* (McGraw-Hill, New York, 1958).
¹⁶T. Maroutian, S. Degen, C. Becker, K. Wandelt, and R. Berndt, *Phys. Rev. B* **68**, 155414 (2003).